FISEVIER

Contents lists available at ScienceDirect

Carbohydrate Polymers

journal homepage: www.elsevier.com/locate/carbpol



Developing chitin nanocrystals for flexible packaging coatings

Tuhua Zhong^a, Michael P. Wolcott^a, Hang Liu^{a,b}, Jinwu Wang^{a,c,*}

- ^a Composite Materials and Engineering Center, Washington State University, Pullman, WA 99164, USA
- ^b Apparel, Merchandising, Design and Textiles, Washington State University, Pullman, WA 99164, USA
- ^c Forest Products Laboratory, U.S. Forest Service, Madison, WI 53726, USA



ARTICLE INFO

Keywords:
Chitin nanocrystals
Coating
Film
Rheology
Laminate
Barrier property

ABSTRACT

This study assessed the applicability of chitin nanocrystals employed in combination with an existing coating material intended for flexible packaging. The 2,2,6,6-tetramethylpiperidine 1-oxyl (TEMPO) oxidized chitin nanocrystals (TOCNs) were applied 1) as an additive in a water-based acrylic resin (WBAR) that was then coated onto the surface of a biaxially oriented polypropylene (BOPP) film, and 2) as a neat layer in multilayered BOPP laminates bonded by a WBAR adhesive layer. The results indicated that the flow behavior and shear viscosity of the TOCN/WBAR system were dependent on TOCN contents. The TOCNs as a dispersed phase in the acrylic resin matrix did not improve the oxygen barrier property of the resulting coated BOPP. By contrast, the neat continuous TOCN coating layer improved the oxygen barrier property of the laminates of BOPP and TOCNs bonded by the acrylic resin, a 44% oxygen transmission rate reduction for a laminate with a 8.33-µm TOCN layer compared to the laminate without a TOCN layer. The inclusion of the TOCNs maintained the optical transparency of the resulting films.

1. Introduction

Much attention has been paid to renewable materials that can be potential to be used as alternative replacements for petroleum-based products. Chitin has gained tremendous attention because it has been recognized as an underutilized biopolymer; this biopolymer exists as a major supporting component in crustaceans, fungi, and insects (Goodrich & Winter, 2007; Kumar, 2000; Nair & Dufresne, 2003). Among various types of chitin, α -chitin is the most ubiquitous, which can be obtained in a large quantity from food waste such as crab, shrimp and lobster shells in the canning industry (Kumar, 2000). Approximate 6 \sim 8 million tonnes of these waste shells are generated annually around the world, and they contain 15 \sim 40% α -chitin (Yan & Chen, 2015). Efficient utilization of chitin as a green component in sustainable products not only can benefit our environment but also can create new added-values of chitin.

Chitin on the nanoscale possesses attractive features such as high specific area, high stiffness, high strength and low density in addition to its nontoxicity, renewability, biodegradability, biocompatibility (Farrán et al., 2015; Ifuku, Morooka, Nakagaito, Morimoto, & Saimoto, 2011; Wu, Zhang, Girouard, & Meredith, 2014). Chitin nanomaterials have been applied as green functional components such as reinforcing and antimicrobial agents for natural and synthetic polymers (Butchosa

et al., 2013; Li et al., 2015; Shams, Ifuku, Nogi, Oku, & Yano, 2011). To our knowledge, little attention has been paid to the applications in coatings intended for packaging applications, especially in water-based coating systems that are more environmentally friendly than solventbased coating systems. Mechanical properties and other performance of water-based coatings are often inferior to those of solvent-based coatings (Tan et al., 2016). The incorporation of nanomaterials from polysaccharides to water-based coating systems could improve mechanical performance while maintaining optical transparency (Grüneberger, Kunniger, Zimmermann, & Arnold, 2014; Tan et al., 2016; Trovatti et al., 2010). TEMPO-mediated oxidation followed by mechanical disintegration can yield water-dispersible TEMPO-oxidized chitin nanocrystals (TOCNs) while retaining high crystallinity (Fan, Saito, & Isogai, 2008). Water-dispersible TOCNs with high stiffness and strength might serve as a potential reinforcing and barrier component in water-based coating systems.

Biaxially oriented polypropylene (BOPP) is a commonly used polymer for food packaging. Poor oxygen barrier properties and low surface energy are two limitations of BOPP (Mirabedini, Arabi, Salem, & Asiaban, 2007; Mokwena & Tang, 2012), which might be overcome by surface coatings with barrier and other functional components or lamination with other barrier polymers (Lange & Wyser, 2003). Conventional oxygen barrier polymers, either in the form of coatings or film

^{*}Corresponding author at: Forest Products Laboratory, U.S. Forest Service, Madison, WI 53726, USA. *E-mail address*: jinwu.wang@usda.gov (J. Wang).

Table 1
Samples codes and constituents s (wt%) of coating formulations.

AR pellets	Ammonium hydroxide solution	Water or TOCNs dispersion	
26	9	65 (water)	
26	9	65 (0.45 wt% TOCNs dispersion)	
26	9	65 (1.36 wt% TOCNs dispersion)	
26	9	65 (2.32 wt% TOCNs dispersion)	
	26 26 26	26 9 26 9 26 9	

laminates for food packaging, are non-degradable and petroleum-based products; common synthetic barrier polymer for packaging include such as polyvinyl alcohol (PVOH), polyvinylidene chloride (PVDC), ethylene vinyl alcohol (EVOH) copolymers (Duan et al., 2013; Hong & Krochta, 2004; Mokwena & Tang, 2012). Sustainable barrier materials based on polysaccharide nanomaterials attract growing interests in recent years. TEMPO-oxidized cellulose nanofibers exhibited excellent oxygen barrier performance when applied to PLA film under the dry environment (Fukuzumi, Saito, Iwata, Kumamoto, & Isogai, 2009). Similarly. TEMPO-oxidized α-chitin nanowhisker coated polylactic acid (PLA) films also exhibited excellent oxygen barrier properties at 0% relative humidity (Fan, Fukuzumi, Saito, & Isogai, 2012). Fukuzumi et al. (2009) and Fan et al. (2012)'s studies indicated that cellulose nanofibers and chitin nanowhiskers are promising barrier materials, even extremely thin coating layer (0.1 \sim 0.4 μ m) to a PLA substrate could impart excellent barrier properties when tested at 0% relative humidity. However, the poor wettability on hydrophobic polymer surfaces and the high sensitivity of either cellulose or chitin nanomaterials to moisture restrict their use in practical applications. For example, hydrophobic polymeric substrates need to be surface-hydrophilized, like plasma-treated, so as to increase the wetting of hydrophilic polysaccharide nanomaterials on their surface (Fan et al., 2012; Fukuzumi et al., 2009). Moreover, surprisingly, chitin nanofiber coated- (~8 µm coating thickness) and cellulose nanocrystal coated (~7 μm coating thickness) PLA films did not exhibit any improved barrier performance whentested at 50% relative humidity (Satam et al., 2018). Satam et al. (2018) also proposed that a spray-assisted layer-bylayer coating of chitin nanofibers and cellulose nanocrystals could overcome adverse effect of moisture to oxygen barrier and improve oxygen barrier properties at high relative humidity. Herein, we attempt to adopt a conventional lamination method that was widely used in food packaging industry, in which hydrophilic barrier materials are wrapped into water-resistant hydrophobic polymeric substrates using a "tie layer" as a bonding (Mokwena & Tang, 2012).

In this paper, the initial attempt was to apply varying TOCN contents to an existing coating system water-based acrylic resin intended for packaging coatings. We investigated their rheological behavior and their coating performance on BOPP substrates including surface energy and oxygen transmission rates. Subsequently, the attempt was to apply TOCNs as a neat barrier layer combined with the existing coating system water-based acrylic resin as a "tie layer" to be laminated with hydrophobic BOPP films so as to address the drawbacks of TOCNs as a dispersed phase in the water-based resin coatings. A multilayered structure was constructed. The effects of the thickness of the TOCN layer on the oxygen transmission rate (OTR) of BOPP laminates were determined. Finally, the optical transparency of water-based acrylic resin/TOCNs coated BOPP films, and BOPP/TOCNs laminates were also determined.

2. Materials and methods

2.1. Materials

Chitin from shrimp shells (powder, technical grade), sodium hypochlorite solution (NaClO, 10–15%, reagent grade), 2,2,6,6-tetramethylpiperidine 1-oxyl (TEMPO, crystal), Formamide (≥99.5%,

BioReagent) and diiodomethane (99%, ReagentPlus) were purchased from Sigma-Aldrich. Sodium bromide (NaBr, crystal, ACS) and ammonium hydroxide solution (NH₄ • OH, 28–30%, ACS) were purchased from EMD Millipore. Sodium hydroxide (NaOH, pellets, certified ACS) and hydrochloric acid (HCl, 36.5–38.0 wt%, certified ACS) were purchased from Fisher Chemical. Water-based acrylic resin (AR) (Joncryl * 678 pellets, molecular weight = 8500) was kindly supplied by BASF company. Terofan ETH57 biaxially oriented polypropylene (BOPP, thickness: 57 μ m) was kindly supplied by Inland Packaging.

2.2. Preparation of chitin nanocrystals

Chitin nanocrystals were prepared from the chitin powder following the method as reported previously (Fan et al., 2008a). Briefly, TEMPO (0.064 g) and sodium bromide (0.4 g) dissolved and mixed in water (100 mL) for 30 min, and then the chitin powder (4.0 g) and the NaClO solution (23.6 g) were added sequentially. The oxidation of chitin occurred at room temperature. The pH of the reaction mixture was maintained at 10.5 by the addition of 0.5 M NaOH solution until no alkali consumption was observed, and then ethanol (8 mL) was added to stop the reaction. The pH was adjusted to 7.0 with HCl solution (0.5 mol/L). The resulting TEMPO- oxidized chitin (TOC) was washed by successive centrifugation and was further disintegrated by an ultrasonic probe (Branson Ultrasonics, USA) for 100 min to obtain a TOCNs dispersion, which stored at $4\,^{\circ}\text{C}$ before use and characterization.

2.3. Preparation of aqueous AR/TOCNs formulations

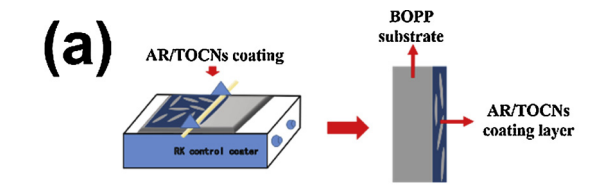
The AR/TOCNs coating formulations were prepared according to Table 1. The TOCN dispersion was adjusted to the desired concentration and then mixed with acrylic resin pellets, which began to dissolve when the neutralizer ammonium hydroxide solution was added. The mixture was further sonicated under an ultrasonic bath until all solids dissolved. A series of AR/TOCNs formulations were prepared with 0, 1, 3, and 5 wt% TOCN loadings based on the weight of the total dry weight of the composite products. These formulations were coded as bare AR, AR/TOCNs1, AR/TOCNs3, and AR/TOCNs5, respectively.

2.4. Fabrication of one-sided AR/TOCNs coated BOPP films

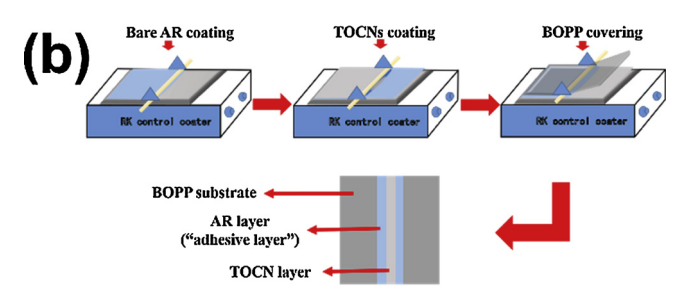
BOPP substrates were coated on one side with aqueous AR/TOCNs formulations with varying TOCN contents (0, 1, 3, and 5 wt%) using a K101 Control Coater (RK Print Coat Instruments, UK). As illustrated in Fig. 1a, approximately 2 mL of a formulation was poured onto one end of the BOPP film. A rod capable of forming 6 µm wet thickness was placed right above the wet formulation and drawn down to the other end of the BOPP film at an even controlled speed of 0.02 m/s. The coatings were air dried under ambient conditions. The samples were labeled as bare AR-BOPP, AR/TOCNs1-BOPP, AR/TOCNs3-BOPP, and AR/TOCNs5-BOPP, corresponding to four TOCN contents, respectively.

2.5. Fabrication of multilayered BOPP/TOCNs laminates

A series of BOPP-AR-TOCNs-AR-BOPP laminates were fabricated as illustrated in Fig. 1b. This film structure was designed to reduce moisture susceptibility of the TOCN layer by sandwiching it within



AR/TOCNs coated BOPP film preparation



BOPP-AR-TOCNs-AR-BOPP laminate preparation

Fig. 1. Schematic diagrams of the preparation of (a) one-sided AR/TOCNs coated BOPP films and (b) multilayered BOPP-AR-TOCNs-AR-BOPP laminates.

moisture resistant BOPP. One BOPP substrate was first coated with the bare AR formulation as an "adhesive layer" and dried The neat TOCNs dispersion of 2 wt% was then coated onto the surface of the AR coating layer with wet thickness being controlled through different rods to be 0, 12, 40 and 100 µm, respectively, and was dried overnight. For preparing laminates, laid the dry TOCN coated BOPP on the coater with the TOCN layer up, poured the calculated amount of the bare AR resin uniformly along one end, placed the other BOPP film on the top of the resin, applied the resin with the rod on the top of the BOPP film and drew down to the other end at an even controlled speed of 0.02 m/s (Fig. 1b). After forming BOPP laminates, the samples were dried in ambient environment for 3 days before characterization. Based on the wet thickness of the TOCN coating layer (0, 12, 40, and 100 μm), the multilayered laminates were coded as BOPP-AR-TOCNs0-AR-BOPP, BOPP-AR-TOCNs40-AR-BOPP, BOPP-AR-TOCNs12-AR-BOPP, BOPP-AR-TOCNs100-AR-BOPP, respectively.

2.6. Scanning electron microscopy (SEM)

Surface morphology of the chitin powder, TOC, neat TOCN coating layers, and the cross-sectional morphology of the laminates was observed with an FEI Quanta 200 F SEM instrument (FEI company, USA) at 20 kV. The samples were coated with platinum using the sputtering process before the SEM analysis.

2.7. Transmission electron microscopy (TEM)

The morphology of the TOC and TOCNs was observed with an FEI Tecnai G2 20 Twin TEM instrument (FEI company, USA) operating at 200 kV. One drop of diluted dispersions was dropped onto a Formvar/carbon coated copper grid, and then one drop of 1% uranyl acetate negative stain was added. The sample on the grid was dried overnight before the TEM analysis.

2.8. Ultraviolet-Visible (UV-vis) spectrophotometer

The light transmittance of the TOC and TOCNs dispersions, and the series of one-sided AR/TOCNs coated BOPP films, and BOPP-AR-TOCNs-AR-BOPP laminates were scanned from 200 nm to 700 nm with a Lambda-25 UV–vis spectrophotometer (PerkinElmer, USA).

2.9. Zeta potential

The zeta potential of the TOCNs in water (concentration: 0.02~wt%, pH = 8) was measured at 20 °C using Nano-Zetasizer (Malvern Instruments, UK).

2.10. Fourier transform infrared spectroscopy (FTIR)

The FTIR spectra of the chitin powder and freeze-dried TOCNs were recorded using a Nicolet Nexus 670 FTIR spectrometer (Thermo Scientific, USA) under the transmission mode from $4000\,\mathrm{cm}^{-1}$ to $400\,\mathrm{cm}^{-1}$ with a $4\,\mathrm{cm}^{-1}$ resolution and 64 scans. Thin sample/potassium bromide (KBr) pellets (Sample-to-KBr ratio: 1/100) were prepared prior to the FTIR analysis.

2.11. X-ray diffraction (XRD)

The XRD patterns of the chitin powder and freeze-dried TOCNs were recorded using an X-ray powder diffractometer (Miniflex 600, Rigaku, Japan) with a Cu K α X-ray source (λ =0.1548 nm) at 40 kV and 15 mA. Crystallinity index (CrI) was estimated from the intensity I_{110} of the plane (110) diffraction peak and the intensity $I_{amorphous}$ at 2 θ = 16.0°. Crystallinity index was calculated using the empirical equation CrI = $(I_{110} - I_{amorphous})/I_{110}$ (Zhang, Xue, Xue, Gao, & Zhang, 2005).

2.12. Rheological behavior measurement

The shear viscosity of the AR/TOCNs formulations was measured at 20 °C in the flow mode by varying the shear rate from 0.01 to 1000 1/s with a Discovery HR-2 parallel plate rheometer (TA Instruments, USA) with the steel plates of the diameter of 25 mm and the gap of 1 mm. The storage modulus G' and loss modulus G'' of the coating formulations as a function of angular frequency ($\omega=1$ –100 rad/s) were measured under the oscillatory test in the linear viscoelastic range of the samples ($\gamma=0.02\%$).

2.13. Contact angles and surface energy measurements

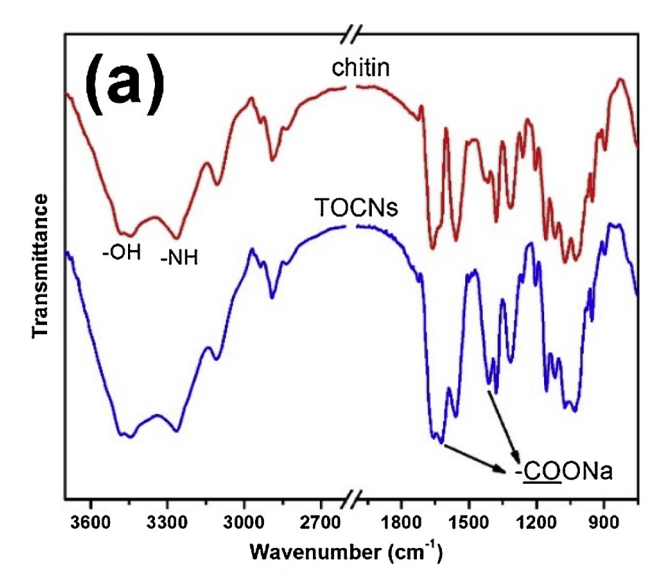
The contact angles of the surfaces of the BOPP and the coating layers were measured by a VCA Optima Video Contact Angle System (AST Products Co., USA). The measurements of the contact angles were performed at room temperature with two polar liquids (water and formamide) and one apolar liquid (diiodomethane). The calculation of surface energy was performed by the SE-2500 surface energy (dyne/cm) software in the instrument provided by the manufacturer.

2.14. Oxygen transmission rate (OTR) measurement

The OTR was measured using a Mocon OX-TRAN 1/50 test system (MOCON, USA) at $20\,^{\circ}\text{C}$ and 50% relative humidity. The coulometric sensor measured oxygen (100%) transmitting through the films or laminates with a surface area of $50\,\text{cm}^2$. The measurements were conducted in duplicate.

2.15. Thickness measurement of neat TOCN coating layers and the laminates

The thickness of the neat TOCN coating layers and the laminates were measured based on cross-sectional SEM images of the samples. Twenty points were measured by ImageJ software for each sample to determine the thickness. The dry thickness of the neat TOCN coating layers and the total thickness of the laminates are presented in Table S1.



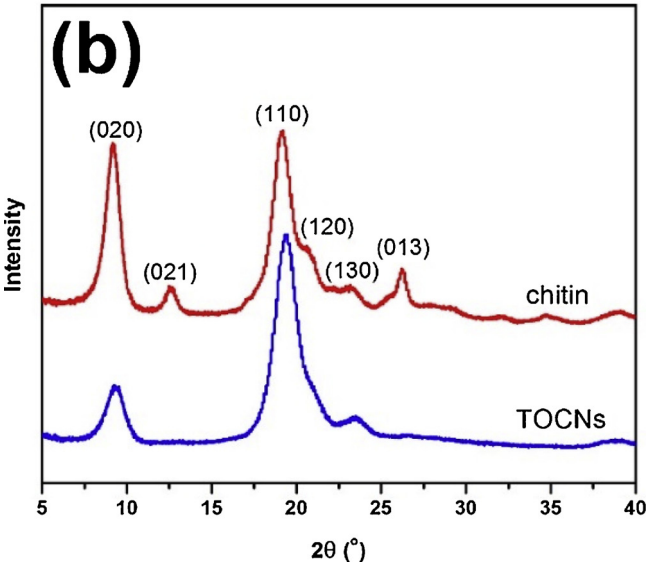


Fig. 2. (a) FTIR spectra and (b) XRD patterns of raw chitin powder and freezedried TOCNs.

3. Results and discussion

3.1. Characteristics of TEMPO-oxidized chitin nanocrystals

The conversion of some hydroxyl groups to carboxyl groups was confirmed by the FTIR spectra of the raw chitin and TOCNs. As shown in Fig. 2a, two strong bands for the chitin observed at 1662 cm⁻¹ and 1558 cm⁻¹ were ascribed to the stretching of C=O in the amide I and the superposition of C-N stretching and NH- bending in the amide II, respectively (Cárdenas, Cabrera, Taboada, & Miranda, 2004; Rinaudo. 2006). The shoulder at 1636 cm $^{-1}$ is a unique characteristic band for α chitin (Rinaudo, 2006), which is not found in β -chitin. The magnitude of absorption bands at 1623 cm⁻¹ and 1412 cm⁻¹ increased considerably for the TOCN sample compared to the untreated sample, which was attributed to the conversion of more C6-hydroxyl groups to carboxylate groups on the surfaces of chitin nanocrystals during the TEMPO oxidation. The band at 1623 cm⁻¹ corresponded to asymmetric stretching of sodium carboxylate groups (-COO Na +), and the band at 1412 cm⁻¹ was assigned to symmetric stretching of carboxylate groups (Fujisawa, Okita, Fukuzumi, Saito, & Isogai, 2011). After protonation, the band due to C=O stretching of sodium carboxylate groups at around $1623~{\rm cm}^{-1}$ was shifted to $1738~{\rm cm}^{-1}$ for the TOCNs containing carboxyl groups (—COOH), as shown in Fig. S1, further confirming the formation of the carboxylate group in the TOCN products.

As illustrated by diffractograms in Fig. 2b, the crystalline structure of chitin might be slightly altered or enhanced after the chitin powder was transformed to the freeze-dried TOCNs. The original chitin powder sample exhibited a typical crystalline structure of α -chitin. Its six characteristic peaks were located at $2\theta = 9.2^{\circ}$, 12.6° , 19.2° , 20.5° , 23.4 $^{\circ}$, and 26.3 $^{\circ}$, which corresponded to (020), (021), (110), (120), (130) and (131) crystallographic planes, respectively (Duan et al., 2013). The peak intensity of crystallographic planes (020) was apparently decreased after the TEMPO oxidation, which is in good agreement with the literature (Fan et al., 2008a). The disappearance of peaks of (021) and (013) might indicate these crystallographic planes were altered during the preparation of chitin nanocrystals. Based on the calculation from the intensity of the (110) crystallographic plane and the intensity of the amorphous phase at $2\theta = 16^{\circ}$ (Zhang et al., 2005), the CrI of the chitin powder was $88.1 \pm 1.5\%$. Although the peak intensity of several crystallographic planes decreased or even disappeared, the CrI of the TOCNs was maintained at a high level at 90.2 \pm 1.1%. There is no statistical difference in the CrI of chitin and TOCN (p = 0.24 > 0.05). The almost unchanged CrI might be ascribed to the removal of amorphous regions from the chitin during the TEMPO oxidation, which offset the decrease or the removal of some crystalline planes.

The microscopic image (Fig. 3a) exhibits diverse surface features of a raw chitin particle, which originate from the microfibrillar structure of chitin. Filament-like chitin microfibrils were clearly revealed after the TEMPO oxidation treatment followed by the freeze-drying, as evidenced by Fig. 3b, c. As can be seen from Fig. 3d, the mechanical disintegration was a crucial step to separate networked microfibrils into individual nanocrystals, which had an average diameter of 8 nm and an average length of 147 nm. The TOCNs dispersion exhibited the flow birefringence under the observation between crossed polarizers (the inset of Fig. 3d), suggesting that rod-like chitin nanocrystals had the optically anisotropic property due to the unidirectional self-orientation of the nanocrystals (Fan et al., 2008a; Fan, Saito, & Isogai, 2008; Liu, Chen, Yue, Chen, & Wu, 2011).

Fig. 4a shows the light transmittance obtained by the UV-vis measurement. The TOCNs dispersion had the transmittance of higher than 88% above 600 nm while the TOC dispersion without ultrasonic treatment exhibited only 5% transmittance. The transparency of chitin nanocrystals is important for their potential use in transparent packaging coatings, films, and laminates because of transparent packaging is informative to consumers at the time of purchase. It is noticeably evident that phase separation between unmodified raw chitin particles and acrylic resin (Fig. 4b), because of the insolubility and indispersibility of chitin particles in water. By contrast, the TOCNs were found compatible with the water-based acrylic resin; the formulations, comprising TOCNs and acrylic resin, were stable as seen in Fig. 4c. The zeta potential of the diluted TOCNs at pH 8 was $^-$ 66.2 \pm 3.6 mV; the negative charges on TOCN surfaces were ascribed to anionic carboxylate groups. Electrostatic repulsion among TOCNs might play a crucial role in promoting well-dispersed chitin nanocrystals in the water-based acrylic resin, vielding stable formulations.

3.2. Rheological behaviors of AR/TOCNs formulations

The TOCNs altered the flow behavior of the water-based acrylic resin. As displayed in Fig. 5a, both the bare AR formulation and the AR formulation with low TOCN content (1 wt%) exhibited almost Newtonian behavior: The viscosity remained almost unchanged with varying shear rates. In addition, it is noted that the shear viscosity was not measurable at the low shear rates for the bare AR formulation and AR/TOCNs1 formulation because of the insensitivity of the rheometer. A more rigid network structure formed at the higher TOCN content (3

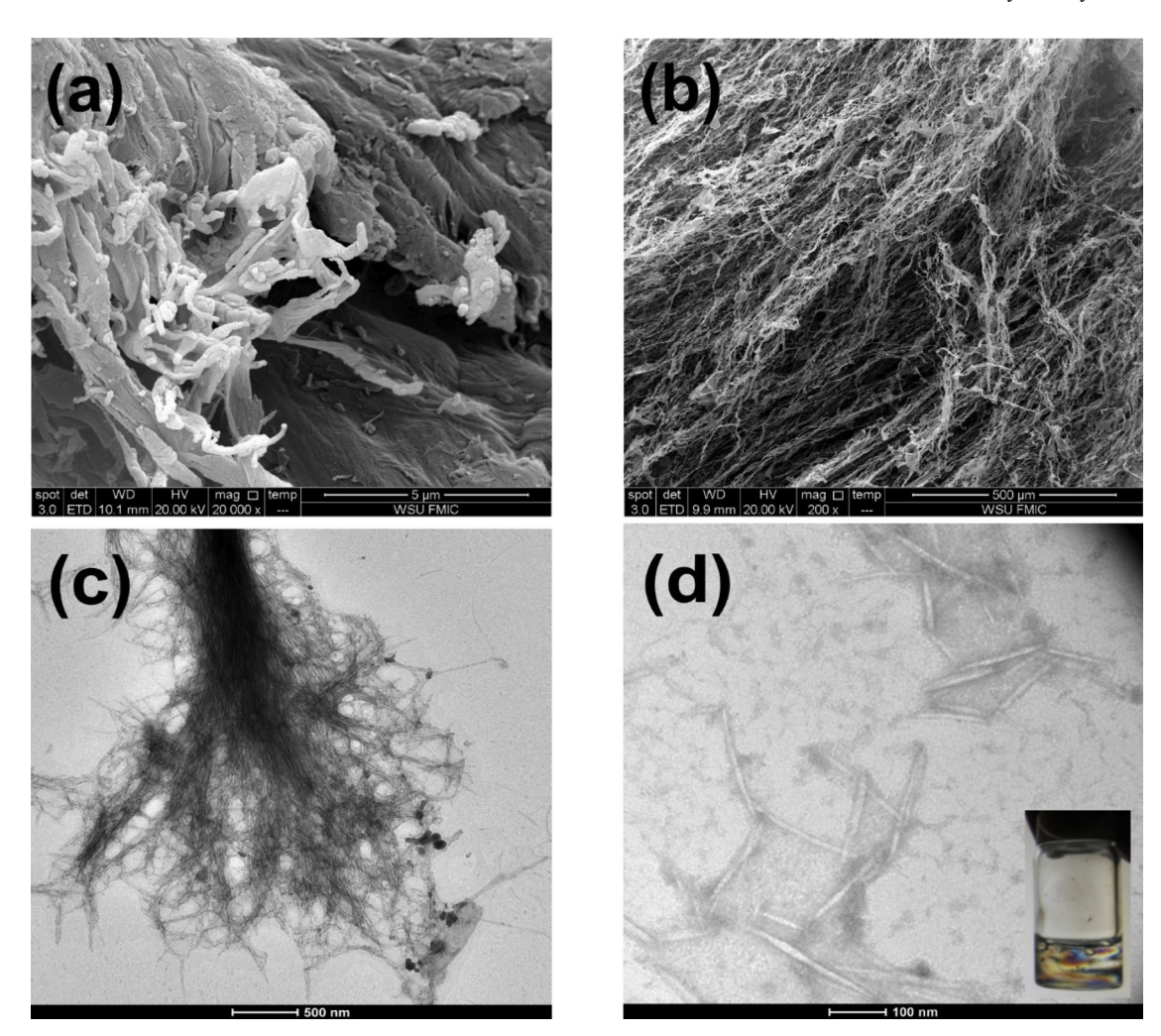


Fig. 3. SEM images of the morphologies of (a) a raw chitin particle and (b) freeze-dried TOC; TEM images of the morphologies of (c) TOC (scale bar = 500 nm) and (d) TOCNs in water (scale bar = 100 nm), inset: TOCNs dispersion observed between crossed polarizers.

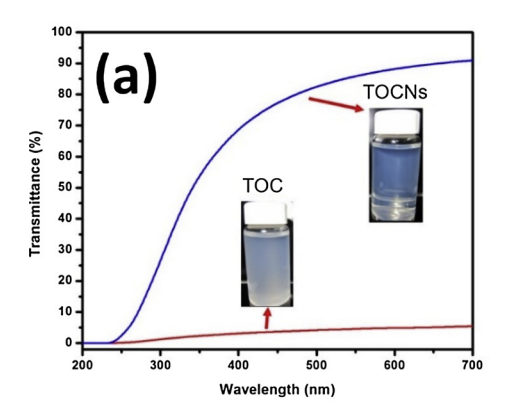
or 5 wt%) resulting in typical shear thinning flow behavior. With increasing shear rate, the viscosity decreased because the network was disrupted (Liu et al., 2011). An evident viscosity plateau in the range from 1 to 5 rad/s appears in the viscosity-shear rate curve of the AR/ TOCNs3 formulation was a similar plateau that was also observed in those of formulations containing other polysaccharide nanofibers or nanocrystals. It was explained that the nanofibers with high aspect ratio might reach a stable network structure resisting the change of shear stress during the plateau period (Iotti, Weiby, Moe, & Lenes, 2011; Li et al., 2015), or that the nanocrystals were induced by shearing to form an ordered network structure hindering the viscosity reduction during that period (Liu et al., 2011). The plateau in this research might be ascribed to be the latter one because of the lower aspect ratio of nanocrystals. As shear rate continued to increase, the ordered network might be broken down again, thereby leading to the decrease in the viscosity. A similar plateau was also found in the AR/TOCNs5 formulation but less pronounced. Fig. 5b shows the viscosity of the acrylic resin coating systems linearly increased with increasing TOCN content at the moderate or high constant shear rates; the effect of the content was smaller at the higher constant shear rate. The increasing likelihood of the hydrogen bonding and Van der Waals forces among TOCNs and acrylic resin molecules with increasing content, might result in the formation of more rigid network structure, thereby leading to the increase in viscosity of coating systems(Grüneberger et al., 2014; Li et al., 2015; Liu et al., 2011).

The dynamic viscoelastic behavior of the water-based acrylic resin

was also altered with the addition of TOCNs. The storage modulus G^{\prime} and loss modulus G " of the formulations containing TOCNs were measured in the frequency sweep mode in the linear viscoelastic (LVE) region because in LVE region applied stresses are insufficient to cause structural breakdown of the structure, and thereby microstructural properties can be measured (Yılmaz, Cheaburu, Gülümser, & Vasile, 2011). Since the low viscosity of the bare AR formulation and AR/ TOCNs1 formulation and the sensitivity of rheometer, the minimum shear strain in the linear viscoelastic region could not be obtained. Fig. 5c shows the storage modulus G' and loss modulus G'' of the AR/ TOCNs3 and AR/TOCNs5 formulations. The AR/TOCNs5 formulation exhibited solid-like (elastic) behavior at low angular frequencies as evidenced by the G' > G". The elastic behavior involves the formation of a network structure (Peressini, Bravin, Lapasin, Rizzotti, & Sensidoni, 2003; Yılmaz et al., 2011). The intersection point of the G' and G curves, indicates the transition to the rubbery state in which the formulation exhibits liquid-like (viscous) behavior. The AR/TOCNs5 formulation had the intersection point at a higher frequency than the AR/ TOCNs3 formulation. It also had a higher storage modulus along with the whole angular frequency range because of its higher TOCN content. The results indicate that the TOCNs have the potential for tailoring the rheological and mechanical properties of water-based coating systems.

3.3. The surface energy of AR/TOCNs coating layers

The surface energy of acrylic resin coating layers was enhanced



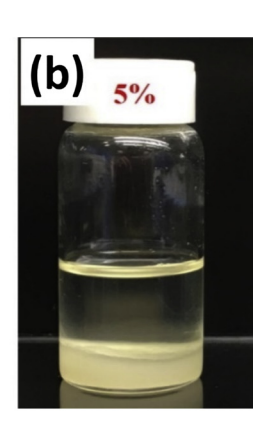


Fig. 4. (a) UV–vis spectra of TOC and TOCNs dispersions (0.9 wt%) and their corresponding photographs (insets); (b) photograph of water-based acrylic resin containing unmodified raw chitin particles (5 wt%); (c) photographs of water-based acrylic resin formulations with various TOCN contents (0, 1, 3 and 5 wt%) (Photos taken after one-month storage of the samples).

(c) 0% 1% 3% 5%

after the incorporation of the hydrophilic TOCNs that had higher surface energy. Table 2 presents the contact angles data and calculated surface energy. The neat TOCN layer had the highest surface energy (58.2 dyn/cm) because of a large number of hydroxyl groups ($^-$ OH) and carboxylate groups ($^-$ COO $^-$) on the TOCN surfaces. The surface energy of the acrylic resin coating layers was increased with increasing TOCN content in the coatings. The surface energy was brought up to 53.9 dyn/cm in the coating layer containing 5 wt% TOCNs in comparison to 51.8 dyn/cm for the AR layer without TOCNs. It is believed that hydrophilic components to the coating layers may contribute to the increase in surface energy because the excessive free hydroxyl and polar groups occur at the solid/air interface (Cozzolino, Campanella, Türe, Olsson, & Farris, 2016).

3.4. Oxygen transmission rate (OTR)

The TOCNs as the dispersed phase in the acrylic resin matrix did not improve the oxygen barrier property. Conversely, the addition of TOCN as the functional filler resulted in the poorer oxygen barrier property of the AR/TOCNs coated BOPP films. Fig. 6a shows that bare AR coating onto BOPP film slightly decreased the OTR in comparison to that of the uncoated BOPP substrate, suggesting that AR has somewhat barrier property. However, with the addition of TOCN into AR coating layer, all the OTR values were higher than that of the bare AR coated BOPP film, indicating that the incorporation of TOCNs into the AR coating layer was detrimental to barrier properties. It could be speculated that the dispersion of chitin nanocrystals in the AR matrix might prevent acrylic molecules from forming a compact structure after water evaporation, which might result in easier penetration of oxygen molecules through the AR/TOCNs interfaces, and thus leading to the increased OTR. The increase in the surface energy of AR coating layer with the TOCN addition might in part account for the reduction in the barrier properties because of the increased sensitivity to moisture when tested at 50% relative humidity.

Although TOCNs as a dispersed phase in the AR matrix exhibited the

incapability of oxygen barrier, we attempted to investigate the oxygen barrier capability of TOCNs when applied as a continuous phase on the substrate. Since there was a considerable discrepancy in surface energy between the continuous TOCN layer and BOPP substrate as listed in Table 2, the acrylic resin was used as an "adhesive layer" between them. Polysaccharides are well known for their high sensitivity to moisture because of their hydrophilic characteristic (El Miri et al., 2015). When these polysaccharide-based films or coatings were exposed at high relative humidity, the plasticizing effect of water could lead to increasing the polymer chain mobility and creating new spaces for permeation of gas molecules (Aulin, Gallstedt, & Lindstrom, 2010; Duan et al., 2013). To address this issue, the multilayered structure was constructed with the TOCN layer as the core protected by water-resistant BOPP as the skins bonded by the acrylic resin (Fig. 1b).

Fig. 6b and c show the OTR and oxygen permeability (OP) of the multilayered BOPP/TOCNs laminates, respectively. The TOCNs as a continuous phase on the substrate did exhibit the capability of oxygen barrier. The OTR of the BOPP/TOCNs laminates decreased with increasing wet thickness of the TOCN layer. The 12- μm wet thickness (dry thickness: $\sim 0.86~\mu m$) did not differ statistically in OTR from that without it. The 40- μm wet thickness (dry thickness: $\sim 5.48~\mu m$) decreased the OTR significantly to $226.2~cm^3/m^2/24~h$ (OP: $269.8~cm^3~\mu m/m^2/day/kPa$). The $100~\mu m$ wet thickness (dry thickness: $\sim 8.33~\mu m$) decreased the OTR to $165.7~cm^3/m^2/24~h$ (OP: $203.8~cm^3~\mu m/m^2/day/kPa$), which is 44.1% OTR reduction (40.5% OP reduction) compared with the BOPP laminate without a TOCN layer. The higher wet thickness might lead to the formation of a thicker and more close-packed structure of the TOCN layer, thus better hinder oxygen transmission.

It is reported that rod-like polysaccharide nanocrystals often exhibit a self-organization phenomenon in water, for example, cellulose nanocrystals align along a vector to form stacked planes; the structure of the stacked planes was preserved after water evaporation (Habibi, Lucia, & Rojas, 2010; Liu et al., 2011). The rod-like TOCNs developed in this research also exhibited a similar self-organization phenomenon,

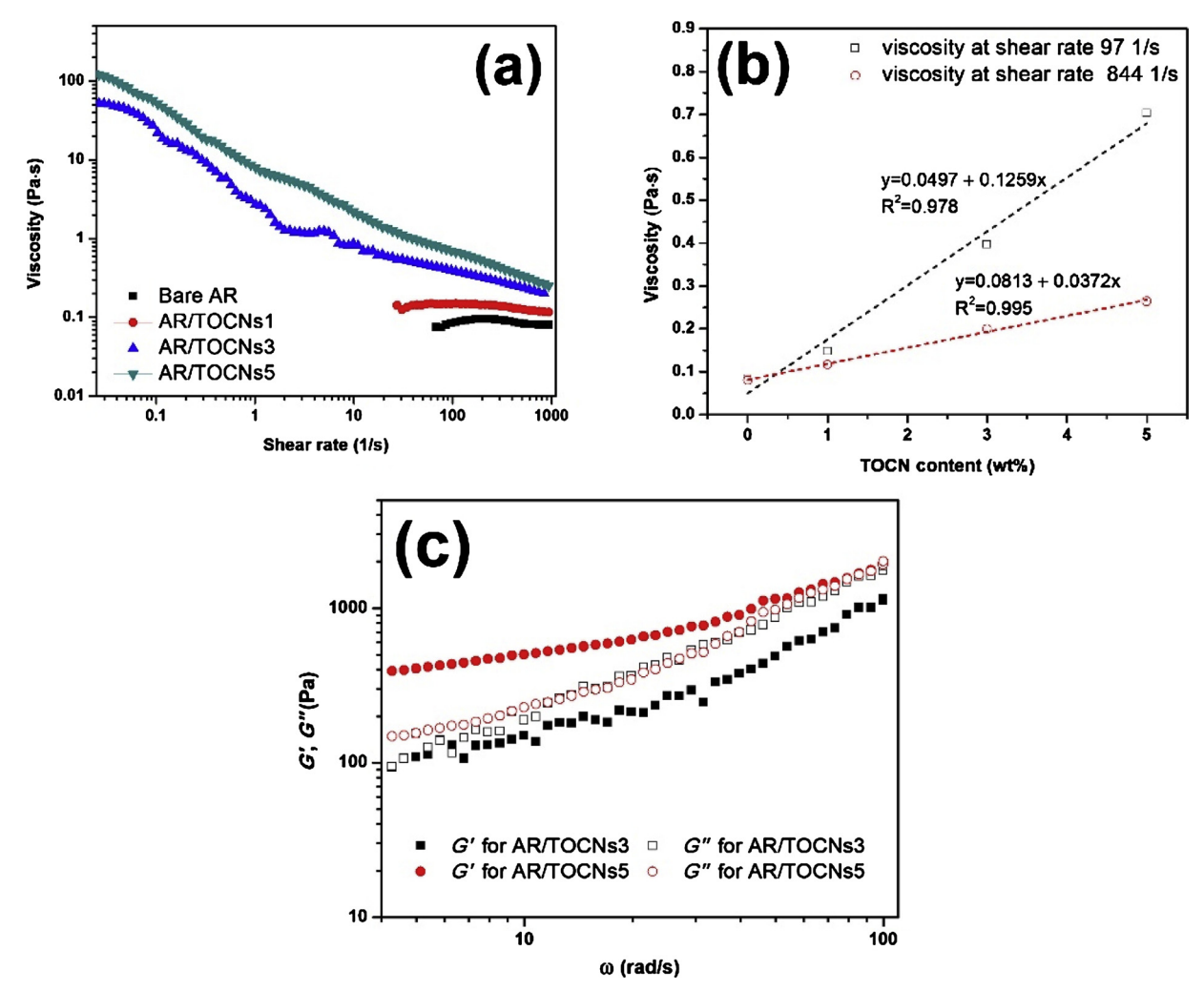


Fig. 5. (a) shear viscosity as a function of shear rate, (b) shear viscosity as a function of TOCN contents at two constant shear rates; (c) storage modulus G' and loss modulus G' as a function of angular frequency G.

Table 2
Contact angles and surface energy.

Surface	θ _{water} (°)	θ _{diiodomethane} (°)	$\theta_{ m formamide}$ (°)	Surface energy (dyn/cm)
BOPP	62.6 ± 2.3	65.9 ± 0.8	51.3 ± 2.0	40.7 ± 0.9
Bare AR	63.0 ± 1.0	37.1 ± 0.8	26.2 ± 1.8	51.2 ± 0.5
TOCNs	43.7 ± 0.9	35.8 ± 1.8	9.5 ± 1.9	58.2 ± 0.5
AR/TOCNs1	62.7 ± 0.8	36.6 ± 1.4	24.2 ± 1.7	51.8 ± 0.8
AR/TOCNs3	62.2 ± 1.2	36.3 ± 1.4	22.9 ± 1.0	52.4 ± 0.2
AR/TOCNs5	61.7 ± 1.3	33.9 ± 2.2	18.8 ± 2.7	53.9 ± 0.5

which is indicated by the appearance of "fingerprint" patterns in TOCNs dispersion as shown in the inset of Fig. 3d. As can be seen from Fig. 7b, such a stacked plane-like structure (the red arrow pointed) also existed in the TOCNs layer after water evaporation, which is a good agreement with the observation using cellulose nanocrystals as coating material (Satam et al., 2018). The higher wet thickness of TOCNs on the BOPP substrate surface might lead to the increased number of such stacked planes after the removal of water, leading to an increase in the thickness as presented in Table S1, and thus resulting in increasingly tortuous path for oxygen molecules, and eventually enabling the effectiveness of preventing oxygen molecules from penetrating through the laminates. The cross-sectional morphology of the laminates taken by the SEM visually showed the change in neat TOCN layer thickness with increasing the wet coating thickness of TOCN suspensions, as evidenced

in Fig. 7f and g as well.

The formation of the more close-packed structure of TOCN layer at higher wet thickness might be another essential factor, which contributed to higher oxygen barrier performance. As mentioned earlier, the 12 µm wet thickness did not increase the oxygen barrier of the resulting BOPP laminate, because this coating thickness was too thin to form a continuous compact layer without defects after water evaporation, needle-like associated TOCNs were still clearly observed; chitin nanocrystal-different zones and even some cracks occurred as shown in Fig. 7a, which facilitated oxygen molecules penetration. It should be noted that these cracks also might be an artifact of SEM imaging, because the TOCN coating layer with made 12-μm wet coating thickness might be too thin to withstand the electron beam during SEM imaging, thus causing the cracking. The higher wet thickness provides relatively close-packed structures with fewer defects after water evaporation, as evidenced by Fig. 7b and c. The morphology profile (needle-like shape) of individual TOCNs, as well as cracks, were not observed in higher wet coating thickness. That might be attributed to that the thicker the TOCN layer, the more lamina the TOCN layer contained creating the effect that the defects in a laminae were most probably masked by the adjacent upper and lower lamina; such a more vertically packed structure could create a more tortuous path to slow oxygen transmission, thus enhancing barrier performance (Aulin et al., 2010).

Although it is encouraging that TOCNs as a continuous phase combined with existing coating material could contribute to the improved oxygen barrier to the packaging laminate, however, it should be

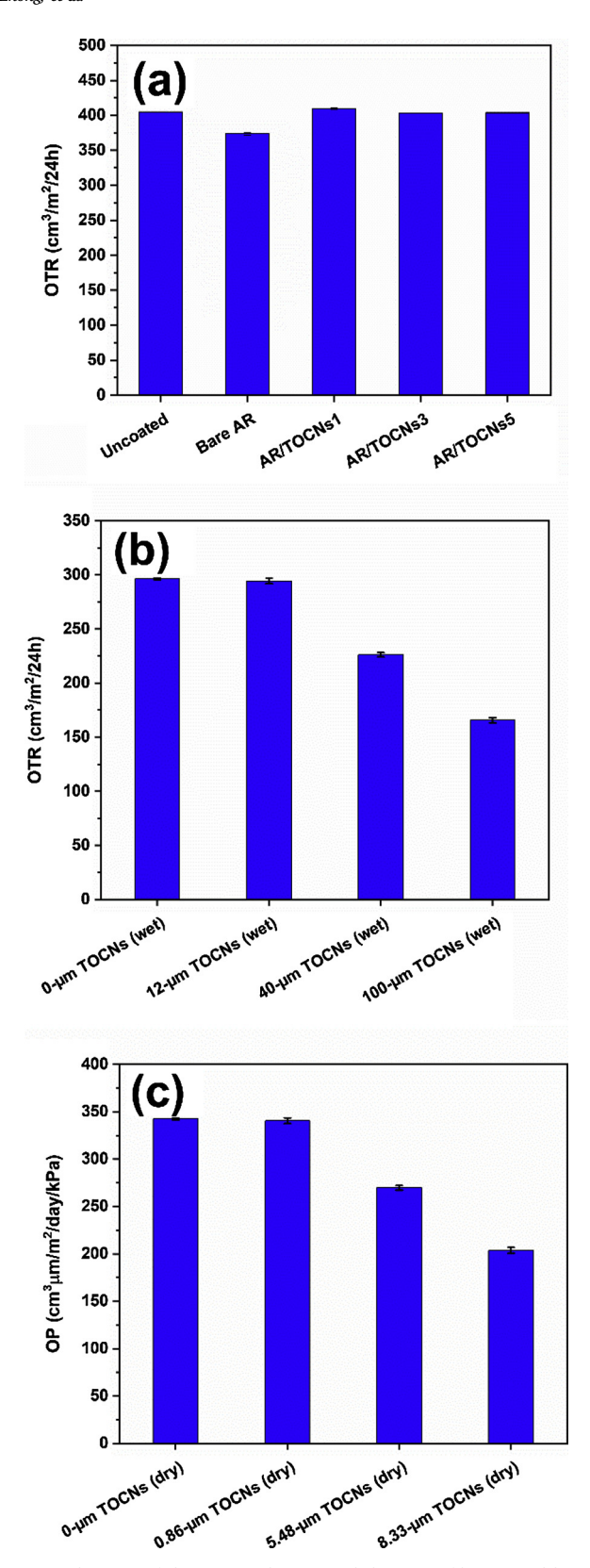


Fig. 6. (a) the OTR of the BOPP substrate and the BOPP films coated by AR/TOCNs with various TOCN contents (0, 1, 3 and 5 wt%); (b) the OTR of the BOPP laminate as a function of TOCN wet coating thickness, and (c) the oxygen permeability (OP) of BOPP laminates as a function of TOCN dry thickness.

noted that the best BOPP laminate with a TOCN layer was not as good barrier performance as conventional barrier materials such as EVOH copolymers. As seen from the cross-sectional morphology of the laminates in Fig. 7f and g, the transverse directional cracks in the TOCN layers were also observed, indicating that the thick TOCN layers are brittle that might be overcome by adding plasticizer like glycerol in the future work. Such cracks might be in part caused by the laminating process, which might reduce the effectiveness of preventing oxygen transmission. However, cracking induced in the SEM sample preparation cannot be excluded.

It is challenging to straightforwardly compare the barrier performance of chitin nanofiber/chitin nanocrystals as a coating on the polymeric film among different studies because of the variation in the characteristics of nano-chitin itself, polymeric substrates, coating methods (spray coating, dip coating, wire wound rod coating, etc), and oxygen permeability test conditions (0% ~ 90% relative humidity). For example, TEMPO-oxidized α-chitin nanowhiskers applied to plasmapretreated (surface-hydrophilized) polylactic acid (PLA) film significantly decreased oxygen permeability from 184 mL µm m⁻² day⁻¹ kPa^{-1} for neat PLA film to 1.01 mL $\mu m\,m^{-2}$ day $^{-1}$ kPa^{-1} for TEMPOoxidized α -chitin nanowhisker coated PLA film (coating thickness ~ 0.1 μm); considering the hydrophilic nature of TEMPO-oxidized chitin nanowhisker, the oxygen permeability was conducted under 0% relative humidity (Fan et al., 2012). Spray assisted layer-by-layer coatings of negatively charged cellulose nanofibers (CNF) and positively charged chitin nanowhiskers (CNW) onto plasma-treated poly(ethylene terephthalate) (PET) were also found to decrease OTR from 38.28 mL $\mbox{m}^{-2}\mbox{day}^{-1}$ for neat PET film to 0.51 mL $\mbox{m}^{-2}\mbox{day}^{-1}$ for CNW/CNF (50 layers) coated PET film under 0% relative humidity (Kim et al., 2019). These studies indicate that the oxygen barrier performance of chitin nanofibers/chitin nanocrystals applied to polymeric films is very promising when they were used under 0% relative humidity. However, it was surprised that layer-by-layer spin coating of anionic cellulose nanofibrils and cationic β -chitin nanofibrils onto PET film did not provide any barrier properties, even under 0% relative humidity, because of the formation of nanoporous structure using spin-coating (Qi, Saito, Fan, & Isogai, 2012). In addition, it was also found that spray coating of neat chitin nanofibers with a much higher thickness of (\sim 8 μ m) or cellulose nanocrystals with a thickness of (\sim 7 μ m) onto the PLA surface did not improve oxygen barrier performance of the chitin nanofiber coated PLA under 50% relative humidity (Satam et al., 2018). Although in our study, TOCN wrapped up in the BOPP laminate by water-based acrylic resin as a "tie layer" did show the improvement on the barrier properties under 50% relative humidity, it was still much lower than commercial barrier packaging products. In the future work, to further improve barrier performance of TOCN in laminates, much work still needs to be systematically investigated on the effects of relative humidity, coating methods, polymeric substrates, the configuration of the laminate, and water vapor transmission rate (WVTR) on barrier performance and of TOCN combined with existing coating materials in laminates.

3.5. Optical transparency

The inclusion of TOCNs in flexible BOPP films, either as an additive in the matrix or as a continuous layer in a laminate did not compromise the optical transparency of the original packaging. Transparency is a desired attribute in the modern food packaging. Fig. 7h shows a representative transparent sample of BOPP/TOCN laminate obtained in our study. The UV-vis spectra in Fig. 8 show that the light transmittance of the AR/TOCNs coated BOPP films and BOPP laminates with a TOCN layer was almost unchanged due to that the TOCNs were substantially smaller than the wavelengths of visible light (approximately 400–800 nm).

4. Conclusions

The manufactured TOCNs with an average diameter of 8 nm and length of 147 nm and having CrI of 90.2% were well compatible with a

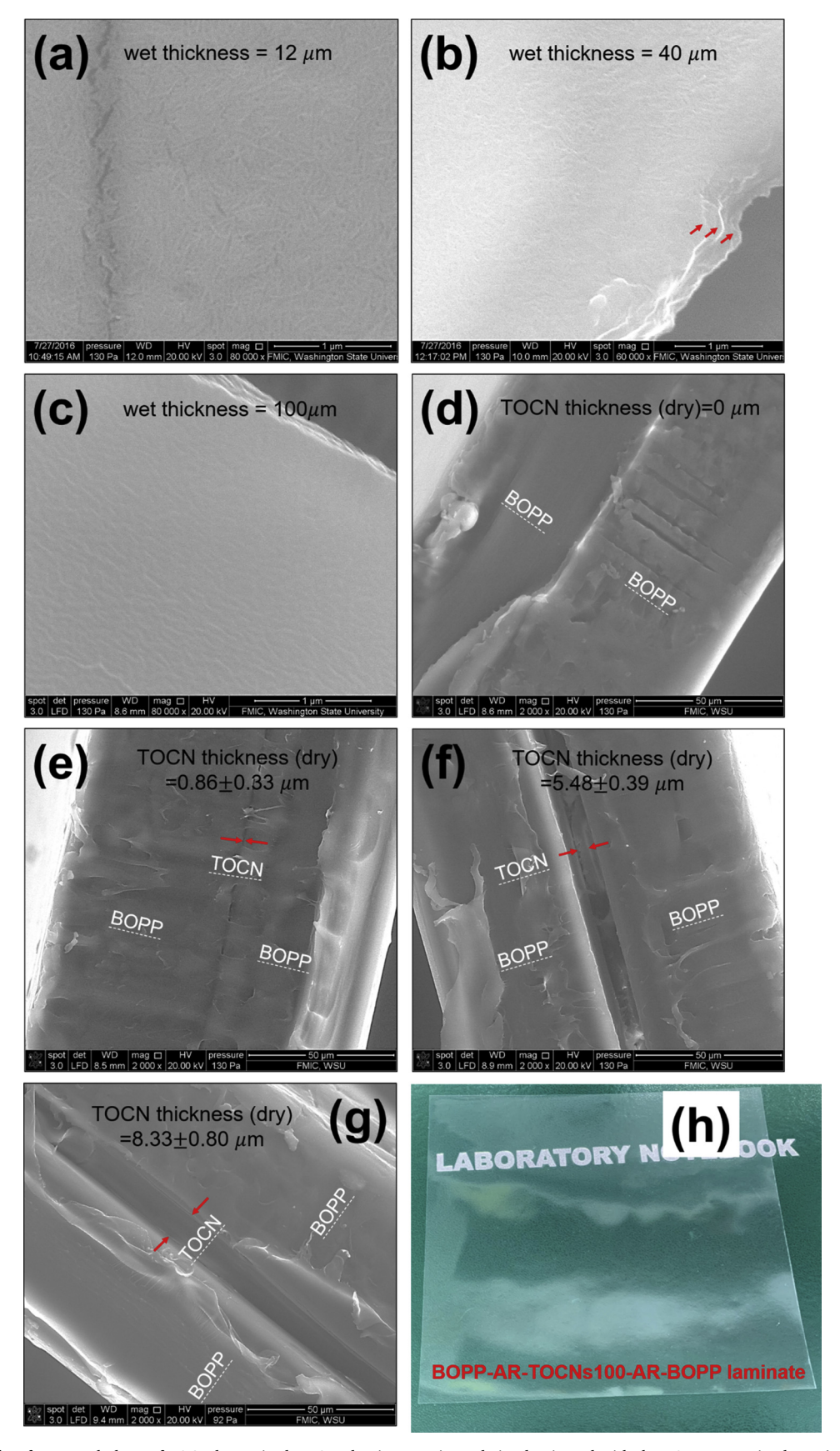


Fig. 7. SEM images of surface morphology of TOCN layers in the BOPP laminates prior to being laminated with the BOPP protective layer (a–c), and cross-sectional morphology of the BOPP laminates with the TOCN layer at various thickness (d–g), and (h) the photograph of a representative transparent BOPP/TOCN laminate.

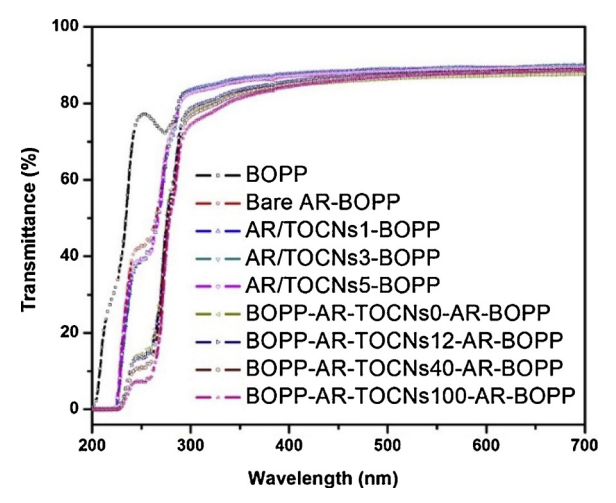


Fig. 8. UV–vis spectra of AR/TOCNs coated BOPP films and multilayered BOPP-AR-TOCNs-AR-BOPP laminates.

water-based acrylic resin (WBAR) and formed stable formulations. When the TOCNs were applied as an additive in the WBAR system, the flow behavior and viscosity were dependent on the TOCN content. The TOCNs enhanced not only material modulus but also enhanced the surface energy of their filled coating layer. However, the TOCNs as dispersed in the acrylic resin matrix did not improve its barrier properties. The TOCNs as a continuous phase can be employed as an oxygen barrier layer, which can be sandwiched by moisture-resistant polymers such as BOPP bonded by a coupling agent such as bare acrylic resins to form multilayered laminates. The thin TOCN layer of an 8.33- μ m dry thickness (based on SEM cross-sectional image) in the core of a laminate could result in 44.1% OTR reduction (40.5% OP reduction) compared with a laminate without the TOCN layer. No matter how the TOCNs were applied in the flexible packaging films, their inclusion did not compromise the optical transparency of the resulting films or laminates. The results demonstrate the potential use of TOCNs as a sustainable material in water-based coating systems for rheology modification and surface energy improvement or as an oxygen barrier layer in packaging. The use of multilayered structures permits the use of different materials in different layers and might open up a way to address the issues of high inherent sensitivity of TOCNs to moisture and their poor compatibility to hydrophobic surfaces in practical applications.

Declaration of Competing Interest

None.

Acknowledgements

This work was supported by the National Science Foundation Industry/University Cooperative Research Center for Bioplastics and Biocomposites (CB²), USA.

Appendix A. Supplementary data

Supplementary material related to this article can be found, in the online version, at doi:https://doi.org/10.1016/j.carbpol.2019.115276.

References

- Aulin, C., Gallstedt, M., & Lindstrom, T. (2010). Oxygen and oil barrier properties of microfibrillated cellulose films and coatings. *Cellulose*, 17, 559–574. https://doi.org/ 10.1007/s/1570.009.93834.
- Butchosa, N., Brown, C., Larsson, P. T., Berglund, L. A., Bulone, V., & Zhou, Q. (2013). Nanocomposites of bacterial cellulose nanofibers and chitin nanocrystals:

- Fabrication, characterization and bactericidal activity. *Green Chemistry, 15*, 3404–3413. https://doi.org/10.1039/c3gc41700j.
- Cárdenas, G., Cabrera, G., Taboada, E., & Miranda, S. P. (2004). Chitin characterization by SEM, FTIR, XRD, and 13C cross polarization/mass angle spinning NMR. *Journal of Applied Polymer Science*, 93, 1876–1885. https://doi.org/10.1002/app.20647.
- Cozzolino, C. A., Campanella, G., Türe, H., Olsson, R. T., & Farris, S. (2016). Microfibrillated cellulose and borax as mechanical, O2-barrier, and surface-modulating agents of pullulan biocomposite coatings on BOPP. Carbohydrate Polymers, 143, 179–187. https://doi.org/10.1016/j.carbpol.2016.01.068.
- Duan, B., Chang, C., Ding, B., Cai, J., Xu, M., Feng, S., ... Zhang, L. (2013). High Strength films with gas barrier fabricated from chitin solution dissolved at low temperature. *Journal of Materials Chemistry A*, 1, 1867–1874. https://doi.org/10.1039/
- El Miri, N., Abdelouahdi, K., Barakat, A., Zahouily, M., Fihri, A., Solhy, A., & El Achaby, M. (2015). Bio-nanocomposite films reinforced with cellulose nanocrystals: Rheology of film-forming solutions, transparency, water vapor barrier and tensile properties of films. Carbohydrate Polymers, 129, 156–167. https://doi.org/10.1016/j.carbpol.2015. 04.051.
- Fan, Y., Fukuzumi, H., Saito, T., & Isogai, A. (2012). Comparative characterization of aqueous dispersions and cast films of different chitin nanowhiskers/nanofibers. *International Journal of Biological Macromolecules*, 50(1), 69–76. https://doi.org/10. 1016/j.ijbiomac.2011.09.026.
- Fan, Y., Saito, T., & Isogai, A. (2008a). Chitin nanocrystals prepared by TEMPO-mediated oxidation of α-chitin. *Biomacromolecules*, 9, 192–198.
- Fan, Y., Saito, T., & Isogai, A. (2008b). Preparation of chitin nanofibers from squid Pen β-chitin by simple mechanical treatment under acid conditions. *Biomacromolecules*, 9(7), 1919–1923. https://doi.org/10.1021/bm800178b.
- Farrán, A., Cai, C., Sandoval, M., Xu, Y., Liu, J., Hernáiz, M. J., & Linhardt, R. J. (2015). Green solvents in carbohydrate chemistry: From raw materials to fine chemicals. Chemical Reviews, 115, 6811–6853. https://doi.org/10.1021/cr500719h.
- Fujisawa, S., Okita, Y., Fukuzumi, H., Saito, T., & Isogai, A. (2011). Preparation and characterization of TEMPO-oxidized cellulose nanofibril films with free carboxyl groups. Carbohydrate Polymers, 84(1), 579–583. https://doi.org/10.1016/j.carbpol. 2010.12.029.
- Fukuzumi, H., Saito, T., Iwata, T., Kumamoto, Y., & Isogai, A. (2009). Transparent and high gas barrier films of cellulose nanofibers prepared by TEMPO-Mediated oxidation. *Biomacromolecules*. 10. 162–165.
- Goodrich, J. D., & Winter, W. T. (2007). α-chitin nanocrystals prepared from shrimp shells and their specific surface area measurement. *Biomacromolecules*, 8, 252–257. https://doi.org/10.1021/bm0603589.
- Grüneberger, F., Kunniger, T., Zimmermann, T., & Arnold, M. (2014). Rheology of nanofibrillated cellulose/acrylate systems for coating applications. *Cellulose*, 21, 1313–1326. https://doi.org/10.1007/s10570-014-0248-9.
- Habibi, Y., Lucia, L. A., & Rojas, O. J. (2010). Cellulose nanocrystals: Chemistry, self-assembly, and applications. Chemical Reviews, 110, 3479–3500.
- Hong, S., & Krochta, J. M. (2004). Whey protein isolate coating on LDPE film as a novel oxygen barrier in the composite structure. *Packaging Technology and Science*, 17, 13–21. https://doi.org/10.1002/pts.634.
- Ifuku, S., Morooka, S., Nakagaito, A. N., Morimoto, M., & Saimoto, H. (2011). Preparation and characterization of optically transparent chitin nanofiber/(meth) acrylic resin composites. Green Chemistry, 13, 1708–1711. https://doi.org/10.1039/c1gc15321h.
- Iotti, M., Weiby, Ø., Moe, S., & Lenes, M. (2011). Rheological studies of microfibrillar cellulose water dispersions. *Journal of Polymers and the Environment*, 19, 137–145. https://doi.org/10.1007/s10924-010-0248-2.
- Kim, T., Tran, T. H., Hwang, S. Y., Park, J., Oh, D. X., & Kim, B. S. (2019). Crab-on-a-tree: All biorenewable, optical and radio frequency transparent barrier nanocoating for food packaging. ACS Nano, 13, 3796–3805.
- Kumar, M. N. V. R. (2000). A review of chitin and chitosan applications. Reactive & Functional Polymers, 46, 1–27. https://doi.org/10.1016/S1381-5148(00)00038-9.
- Lange, J., & Wyser, Y. (2003). Recent innovations in barrier technologies for plastic packaging-a review. *Packaging Technology and Science*, 16, 149–158. https://doi.org/ 10.1002/pts.621.
- Li, M.-C., Wu, Q., Song, K., Lee, S., Qing, Y., & Wu, Y. (2015). Cellulose nanoparticles: Structure – morphology – rheology relationships. ACS Sustainable Chemistry & Engineering, 3, 821–832. https://doi.org/10.1021/acssuschemeng.5b00144.
- Liu, D., Chen, X., Yue, Y., Chen, M., & Wu, Q. (2011). Structure and rheology of nanocrystalline cellulose. *Carbohydrate Polymers*, 84(1), 316–322. https://doi.org/10. 1016/j.carbpol.2010.11.039.
- Mirabedini, S. M., Arabi, H., Salem, A., & Asiaban, S. (2007). Effect of low-pressure O2 and Ar plasma treatments on the wettability and morphology of biaxial-oriented polypropylene (BOPP) film. *Progress in Organic Coatings*, 60, 105–111. https://doi.org/10.1016/j.porgcoat.2007.07.007.
- Mokwena, K. K., & Tang, J. (2012). Ethylene vinyl alcohol: A review of barrier properties for packaging shelf stable foods. Critical Reviews in Food Science and Nutrition, 52(7), 640–650. https://doi.org/10.1080/10408398.2010.504903.
- Nair, G. K., & Dufresne, A. (2003). Crab shell chitin whisker reinforced natural rubber nanocomposites. 1. processing and swelling behavior. *Biomacromolecules*, 4(3), 657–665. https://doi.org/10.1021/bm020127b.
- Peressini, D., Bravin, B., Lapasin, R., Rizzotti, C., & Sensidoni, A. (2003). Starch–Methylcellulose based edible films: Rheological properties of film-forming dispersions. *Journal of Food Engineering*, 59, 25–32. https://doi.org/10.1016/S0260-8774(02)00426-0.
- Qi, Z. D., Saito, T., Fan, Y., & Isogai, A. (2012). Multifunctional coating films by layer-by-layer deposition of cellulose and chitin nanofibrils. *Biomacromolecules*, 13(2),
- Rinaudo, M. (2006). Chitin and chitosan: Properties and applications. Progress in Polymer

- Science, 31, 603-632. https://doi.org/10.1016/j.progpolymsci.2006.06.001.
- Satam, C. C., Irvin, C. W., Lang, A. W., Jallorina, J. C. R., Shofner, M. L., Reynolds, J. R., & Meredith, J. C. (2018). Spray-coated multilayer cellulose nanocrystal—Chitin nanofiber films for barrier applications. ACS Sustainable Chemistry & Engineering, 6(8), 10637–10644.
- Shams, M. I., Ifuku, S., Nogi, M., Oku, T., & Yano, H. (2011). Fabrication of optically transparent chitin nanocomposites. Applied Physics A, Materials Science & Processing, 102, 325–331. https://doi.org/10.1007/s00339-010-5969-5.
- Tan, Y., Liu, Y., Chen, W., Liu, Y., Wang, Q., Li, J., & Yu, H. (2016). Homogeneous dispersion of cellulose nanofibers in waterborne acrylic coatings with improved properties and unreduced transparency. ACS Sustainable Chemistry & Engineering, 4, 3766–3772. https://doi.org/10.1021/acssuschemeng.6b00415.
- Trovatti, E., Oliveira, L., Freire, C. S. R., Silvestre, A. J. D., Neto, C. P., Pinto, J. J. C. C., & Gandini, A. (2010). Novel bacterial cellulose–acrylic resin nanocomposites. Composites Science and Technology, 70(7), 1148–1153. https://doi.org/10.1016/j.

- compscitech.2010.02.031.
- Wu, J., Zhang, K., Girouard, N., & Meredith, J. C. (2014). Facile route to produce chitin nanofibers as precursors for flexible and transparent gas barrier materials. *Biomacromolecules*, 15, 4614–4620. https://doi.org/10.1021/bm501416q.
- Yan, N., & Chen, X. (2015). Don't waste seafood waste: Turning cast-off shells into nitrogen-rich chemicals would benefit economies and the environment. *Nature*, 524, 155–157
- Yılmaz, O., Cheaburu, C. N., Gülümser, G., & Vasile, C. (2011). Rheological behaviour of acrylate/montmorillonite nanocomposite latexes and their application in leather finishing as binders. *Progress in Organic Coatings*, 70, 52–58. https://doi.org/10.1016/ j.porgcoat.2010.10.001.
- Zhang, Y., Xue, C., Xue, Y., Gao, R., & Zhang, X. (2005). Determination of the degree of deacetylation of chitin and chitosan by X-ray powder diffraction. *Carbohydrate Research*, 340, 1914–1917. https://doi.org/10.1016/j.carres.2005.05.005.